ORGANIC CHEMISTRY
FRONTIERS

RESEARCH ARTICLE

Cite this: *Org. Chem. Front.*, 2019, **6**, 2860

Diels–Alder reaction on perylenediimides: synthesis and theoretical study of core-expanded diimides†‡

Nathalie Zink-Lorre, §[a] Azahara Doncel-Giménez,§[b] Enrique Font-Sanchis, [a] Joaquín Calbo, [b] Ángela Sastre-Santos, [a] Enrique Ortí *[b] and Fernando Fernández-Lázaro *[a]

Received 24th May 2019,
Accepted 27th June 2019

DOI: 10.1039/c9qo00682f

rsc.li/frontiers-organic

A one-step reaction for the fusion of aromatic rings to one or both bay areas of perylenediimides using benzynes is presented. Yields as high as 70% for naphthoperylenendiimide **2** and 80% for dibenzocoronenediimide **3** are obtained. The reaction is also carried out using substituted benzynes, heteroaromatic benzynes and substituted perylenediimides. A combined experimental/theoretical approach, based on measuring redox and absorption/emission properties and performing density functional theory calculations, indicates that increasing the π-skeleton of PDIs transversally leads to significant and unexpected changes in the electronic, redox and optical properties. The observed trends are rationalized in terms of molecular orbital topology and overlap according to three different levels of core expansion, and can be used as design principles for obtaining PDIs with improved functionalities.

Introduction

Perylenediimides (PDIs)[1] are important dyes and pigments that are currently investigated for biological[2] and technological applications.[3] They possess outstanding chemical, thermal, optical and electronic properties, which can be finely tuned by attaching a variety of substituents at the different available positions: imido, bay (positions 1, 6, 7, and 12 of the aromatic core) and *ortho* (positions 2, 5, 8, and 11 of the aromatic core).[1g,4] PDIs can also be used as seeds to grow larger aromatic diimide structures, which present a deeper alteration of the molecular properties. Thus, the basic perylene core may be extended by the introduction of additional naphthalene units along the main axis (the longitudinal one) of the PDI structure leading to the rylenediimides, *e.g.* terrylenediimide, quaterrylenediimide, pentarrylenediimide, *etc*. This extension of the aromatic core leads to interesting optical features such as a bathochromic shift and an increase of intensity in the absorption spectra.[5]

There is also the possibility to expand the aromatic core of PDI by introducing extra benzene rings along the transversal or short molecular axis giving rise to coronenediimide (CDI), dibenzocoronenediimide (DBCDI), dinaphthocoronenediimide (DNCDI) and so on (Fig. 1). In this case, moving from PDI to CDI induces a hypsochromic shift of the lowest-energy band in the absorption spectrum.[6] This is an unexpected behavior because an increase in size of the conjugated structure is usually accompanied by a redshift of the absorption. Further extension of the aromatic core of CDI occurs with a bathochromic shift and a decrease of the extinction coefficient in the absorption spectra.[7]

Some synthetic routes have been devised to obtain coronene and core-expanded analogues, which rely on a two-reactions sequence starting from brominated PDIs. Thus, benzoperylenediimide and CDI were prepared by Sonogashira reac-

[a]*Área de Química Orgánica, Instituto de Bioingeniería, Universidad Miguel Hernández de Elche, Avda. de la Universidad s/n, 03202 Elche, Spain. E-mail: fdofdez@umh.es*
[b]*Instituto de Ciencia Molecular, Universidad de Valencia, Catedrático José Beltrán 2, 46980 Paterna, Spain. E-mail: enrique.orti@uv.es*

† Dedicated to Prof. Eugenio Coronado on occasion of his 60th birthday.

‡ Electronic supplementary information (ESI) available: NMR, IR, UV-vis, fluorescence and MS spectra, optimized structures, topologies and energy diagrams of frontier MOs, calculated ionization potentials and electron affinities and calculated Cartesian coordinates. See DOI: 10.1039/c9qo00682f

§ These authors contributed equally to the work.

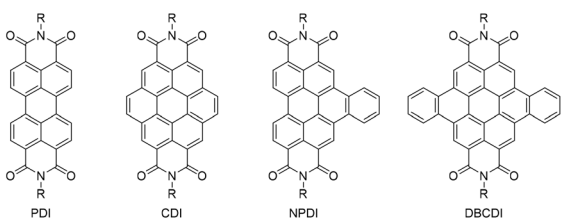

Fig. 1 Core-expanded PDIs.

tion of a terminal alkyne with a (di)bromo-substituted PDI, followed by intramolecular cyclization under strong basic conditions or metal catalysis or reaction with iodine(I) chloride.[6,8]

On the other hand, naphthoperylenediimide (NPDI), DBCDI and π-extended analogues have been synthesized by Suzuki or Stille reaction of an aromatic organometallic on a (di)bromo-substituted PDI, followed by a benzannulation through a palladium-catalyzed process, a Scholl reaction or a phototriggered intramolecular cyclization.[9] In the latter case, it is interesting to note that, surprisingly, Diels–Alder reactions on the naked PDI have not been employed to construct the NPDI and DBCDI skeletons. Although the Diels–Alder reaction has been widely used on perylene,[10] the examples using PDI are limited to some dienes.[10d,11] During the preparation of this manuscript, a communication by Ito, Itami and cols. was reported, where a benzyne-based strategy is employed to fuse aromatic rings onto the bay area of PDI. In their work, the authors use three different 2-(trimethylsilyl)aryl trifluoromethanesulfonates reporting yields of isolated compounds ranging from 15 to 54%.[12]

Herein we present a strategy to obtain core-expanded PDI derivatives by Diels–Alder reaction using different sources of benzyne and starting from unfunctionalized precursors. The scope of the reaction is tested using substituted benzynes and heteroaromatic benzynes. Moreover, the reaction can be carried out with functionalized PDIs, which would result in novel and interesting derivatives. A thorough theoretical study on the effects that core expansion has on the optical and electrochemical properties of the synthesized compounds is performed and correlated with the experimental electrochemical and optical data.

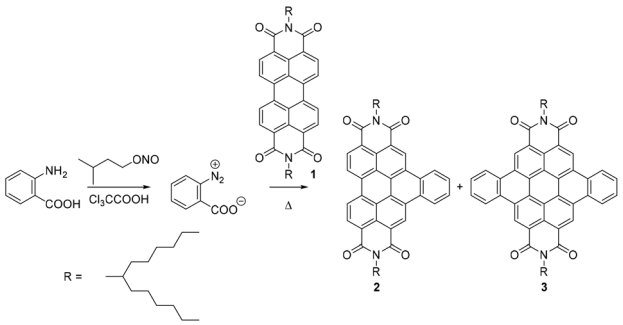

Scheme 1 Core expansion of PDI **1** with anthranilic acid.

Table 1 Selection of conditions for the reaction of anthranilic acid and PDI **1**

Entry[a]	Antranilic acid (mmol)	*V* (mL)	Time (h)	**2** [b] (%)	**3** [b] (%)
1	1	5	24	33	8
2	2	5	24	40	4
3	3	5	24	36	6
4	4	5	24	37	12
5	10	5	24	43	43
6	10	10	24	70	10
7	10	5	36	18	60
8	10	5	18	65	13
9	10	5	12	44	15
10	12	5	24	37	41

[a] Reagents and conditions: PDI **1** (0.2 mmol), anthranilic acid, THF, 70 °C. [b] Yield of isolated, purified products.

Results and discussion

Synthesis of core-expanded PDI derivatives

The formation of the asymmetric NPDI (**2**) or the symmetric DBCDI (**3**) derivative strongly depends on the conditions of the reaction and on the source of benzyne. We studied two different well-known precursors of benzyne: the anthranilic acid and the 2-(trimethylsilyl)phenyl trifluoromethanesulfonate. To set the conditions of the reactions for obtaining either **2** or **3** as major compound, we selected PDI **1** as starting material owing to its high solubility in most organic solvents. The substituent at the imide position does not alter the electronic structure of the PDI.[1]

We first studied the anthranilic acid precursor and, following the procedure previously described,[13] we made it to react with PDI **1** (Scheme 1, Table 1). Due to the limitations in the conditions needed to obtain the benzyne, the solvent selected was tetrahydrofuran and the temperature was set to solvent reflux. Different stoichiometries of the starting compounds were studied (entries 1–5 and 10 in Table 1). The best result was obtained using 10 equivalents of anthranilic acid (entry 5). The effect of time was furthermore investigated (entries 5 and 7–9). Shorter reaction times led to a higher rate of **2** (entry 8), whereas longer times favored the formation of **3** (entry 7). On the other hand, increasing the amount of solvent (entry 6) resulted in a higher yield of NPDI **2**.

In our hands, the best yield of NPDI **2** (70%) and of DBCDI **3** (60%) were obtained using 10 equivalents of anthranilic acid and 10 mL of THF after 24 h for **2**, and using 10 equivalents of antranilic acid and 5 mL of THF after 36 h for **3** (referred to as methods A and B, respectively, from now on). The only byproduct obtained was unreacted starting material **1**.

In a step further, we tested a different precursor for the benzyne, namely 2-(trimethylsilyl)phenyl trifluoromethanesulfonate, which undergoes a fluoride-mediated process to generate the desired intermediate.[10f,g,14] This reagent was previously used to synthesize the DBCDI skeleton.[8e,15] Müllen and col. reacted 1,7-dibromoPDI with 2-(trimethylsilyl)phenyl trifluoromethanesulfonate in the presence of CsF, a phosphine and a palladium catalyst, and they did not try with the bare PDI. On our side, we reacted **1** with the silylated triflate in the presence of fluoride according to Scheme 2. From the different solvents and fluoride sources described in the literature,[10f,16] we selected a mixture of toluene and acetonitrile, which allows dissolving both the fluoride salt and the PDI, and CsF as fluoride source. Based on our previous experience with the anthranilic acid we decided to employ an excess of benzyne, so we started using a 1 : 5 PDI : triflate stoichiometry with an

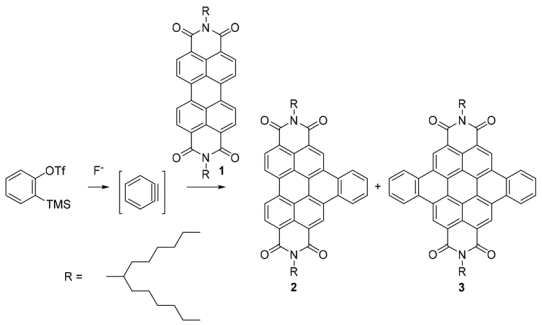

Scheme 2 Core expansion of PDI **1** with 2-(trimethylsilyl)phenyl trifluoromethanesulfonate.

excess of F^- to guarantee the formation of the benzyne. The results are shown in Table 2.

The first attempt (entry 1) afforded 42% yield of **2**. Trying to favor the formation of **3**, we tested the same conditions reducing the volume of solvent (entries 2 and 3) to afford **2** in 70% and **3** in 44% yield. An increase in the proportion of triflate enhanced the yield of **3** to 68% (entries 4, and 5), and even reached 80% yield by allowing a longer reaction time (entry 6).

To test higher temperatures, we changed the solvent to DMF (entry 8) but it resulted in very disappointing yields, probably due to a poor solubility of the reactants. Finally, we tested TBAF as a source of fluoride (entries 9 and 10). In this case, not only the yields of the desired compounds were low (from 0 to 14%), but also, a third unexpected compound, namely 1-hydroxyPDI, was formed (Scheme 3). This reaction has been widely studied in our research group.[4d–g]

Trying to find milder conditions, we tested dry THF as solvent at reflux temperature in combination with CsF and 18-crown-6 (4 : 1 proportion relative to the alkaline ion). In a first attempt (entry 1, Table 3), using 4 equivalents of benzyne and 4 mL of THF, NPDI **2** was obtained in 67% yield after 16 h. When longer reaction times were tried (entries 2 and 4),

Table 2 Selection of conditions for the reaction of 2-(trimethylsilyl) phenyl trifluoromethanesulfonate and PDI **1**

Entry[a]	Benzyne (mmol)	F^- (mmol)	Solvent	**2** [b] (%)	**3** [b] (%)
1	0.5	1	Tol/CH_3CN 1/1, 18 mL	42	0
2	0.5	1	Tol/CH_3CN 1/1, 2 mL	70	28
3	0.5	1	Tol/CH_3CN 1/1, 1 mL	40	44
4	1	1.2	Tol/CH_3CN 1/1, 2 mL	24	57
5	1	1.2	Tol/CH_3CN 1/1, 1 mL	20	68
6[c]	1	1.2	Tol/CH_3CN 1/1, 1 mL	18	80
7	1.5	1.8	Tol/CH_3CN 1/1, 2 mL	52	0
8[d]	0.5	1	DMF, 18 mL	0	0
9[e,f]	0.5	1	Toluene, 4 mL	14	0
10[e,g]	0.5	1	THF, 4 mL	10[h]	0

[a] Reagents and conditions: PDI **1** (0.1 mmol), 2-(trimethylsilyl)phenyl trifluoromethanesulfonate, CsF, 80 °C, 24 h. [b] Yield of isolated, purified products. [c] Reaction time: 36 h. [d] Heated to 150 °C. [e] TBAF from a 1 M solution in THF. [f] Heated to 100 °C. [g] Heated to 70 °C. [h] 26% HO-PDI was also isolated.

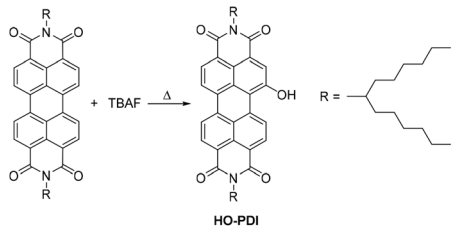

Scheme 3 Hydroxylation of PDI **1**.

Table 3 Selection of the conditions for the reaction of 2-(trimethylsilyl) phenyl trifluoromethanesulfonate and PDI **1** using THF as solvent

Entry[a]	Benzyne (mmol)	CsF (mmol)	*V* (mL)	Time (h)	**2** [b] (%)	**3** [b] (%)
1	0.4	0.4	4	16	67	0
2	0.4	0.4	4	24	40	10
3	0.4	0.4	2	24	50	0
4	0.4	0.4	4	36	40	14
5	0.8	0.8	4	24	25	20
6	1.2	1.2	4	24	20	30
7	1.6	1.6	4	24	36	56
8	1.2	1.2	4	36	24	73
9	1.6	1.6	4	36	42	58

[a] Reagents and conditions: PDI **1** (0.1 mmol), 2-(trimethylsilyl)phenyl trifluoromethanesulfonate, 18-crown-6, 70 °C, THF. [b] Yield of isolated, purified products.

DBCDI **3** started to appear. In this case, reduction of the solvent amount (entry 3) did not result in better yields, so we decided to increase the proportion of the reactants (entries 5–7) and the reaction time (entries 8 and 9). The highest yields finally obtained were 67% for compound **2** (entry 1) and 73% for compound **3** (entry 8).

Considering the results shown in Tables 2 and 3, entries 2 and 6 of Table 2 were chosen as the best conditions for obtaining **2** and **3**, respectively, using 2-(trimethylsilyl)phenyl trifluoromethanesulfonate as precursor of the benzyne. From now on, these conditions will be referred to as methods C and D, respectively.

The scope and applicability of the reaction was furthermore investigated by using functionalized benzynes (Fig. 2, Table 4). First, we reacted 2-amino-5-iodobenzoic acid (Fig. 2a) with **1** under method A conditions obtaining 75% and 16% of the iodine-substituted derivatives NPDI **4** and DBCDI **5**, respectively (Fig. 3). Method B led to 32% of **4** and 56% of **5**.

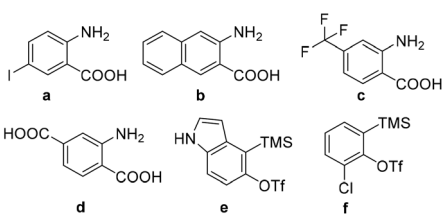

Fig. 2 Benzyne precursors.

Table 4 Reaction of PDI **1** with benzyne precursors **a–f** (Fig. 2)

		Method			
Compound	Benzyne precursor	A (%)	B (%)	C (%)	D (%)
4	**a**	75	32		
5	**a**	16	56		
6	**b**	32	38		
7	**b**	Traces	Traces		
8	**d**	22	28		
9	**c**		22		
10	**c**		Traces		
11	**e**			50	64
12	**f**			35	43

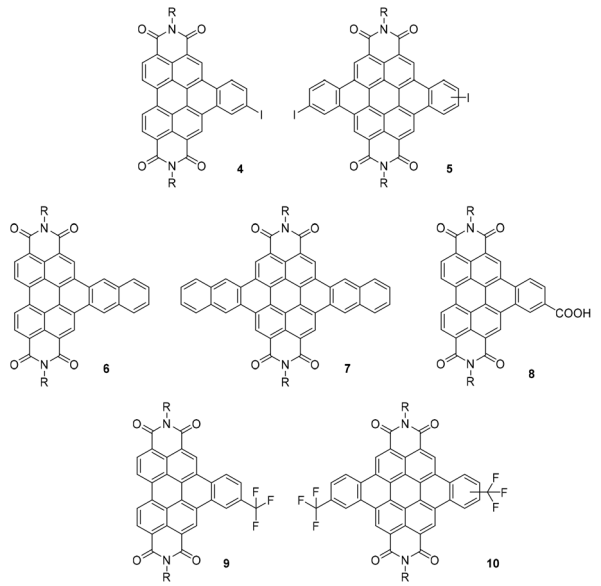

Fig. 3 Functionalized core-expanded PDIs **4–10**.

Methods A and B were then assayed with some other derivatives of the anthranilic acid, namely the 3-amino-2-naphthoic acid (Fig. 2b), the 2-amino-4-(trifluoromethyl)benzoic acid (Fig. 2c) and the 2-aminoterephthalic acid (Fig. 2d). We also conducted methods C and D on two different (trimethylsilyl) aryl triflates: 4-(trimethylsilyl)-1*H*-indol-5-yl trifluoromethanesulfonate (Fig. 2e) and 2-chloro-6-(trimethylsilyl)phenyl triflate (Fig. 2f). The results are shown in Table 4 and Fig. 3.

Table 4 shows that the reaction conditions used in methods A and B are very appropriate for the preparation of compounds **4** and **5** starting from 2-amino-5-iodobenzoic acid. The other anthranilic acid derivatives led to low yields (22–38%) of the Diels–Alder monoadducts **6**, **8** and **9**, and only traces of the diadducts **7** and **10**. Therefore, a specific study of the conditions might be necessary in each single case. For example, compound **7** was only detected by HRMS MALDI TOF, probably due to the propensity of **6** to aggregate owing to its extended π-conjugated structure, which determines the low solubility of **6** in the reaction medium. It is important to note that the synthesis of **9** and **10** was only tried once, using method B. Despite this limitation, **9** was obtained in 22% yield, and the formation of **10** was observed, thus pointing out to the validity of the method. In our hands, compounds **5** and **10** were obtained as a mixture of isomers that could not be resolved by chromatography.

The use of (trimethylsilyl)aryl triflates under methods C and D only led to the preparation of the Diels–Alder monoadducts **11** and **12** (Fig. 4) in moderate to good yields (43–64%).

Finally, we tried the reaction on the already functionalized PDI **13** bearing four 2,6-diphenylphenoxy groups at the *ortho* positions.[4f] Compounds **14** and **15** were obtained in 61% and 7% yields, respectively, using method A, and 58% and 9% yields, respectively, with method B (Scheme 4). Since the low yields for **15** were probably due to the high steric hindrance caused by the bulky substituents, we applied the same procedure on PDI **16**, the precursor of **13** (Scheme 5). Method B afforded compound **17** in 86% yield, which was reacted with diphenylphenol to generate DBCDI **15** in 89% yield (overall yield 77% from **16**).

The synthesis of **15** shows the potential of this methodology. The main limitation appears when the monoadduct is not soluble enough, thus preventing the possibility of a second Diels–Alder reaction.

Electrochemical properties

Fig. 5 compares the redox behaviour recorded for compounds **1–3**, **6** and **11** using differential pulse voltammetry (DPV), and Table 5 collects the oxidation and reduction potentials together with the energies estimated for the highest-occupied

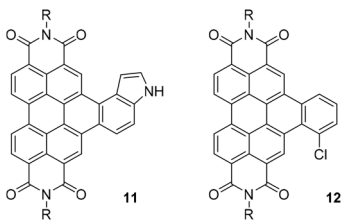

Fig. 4 NPDIs **11** and **12**.

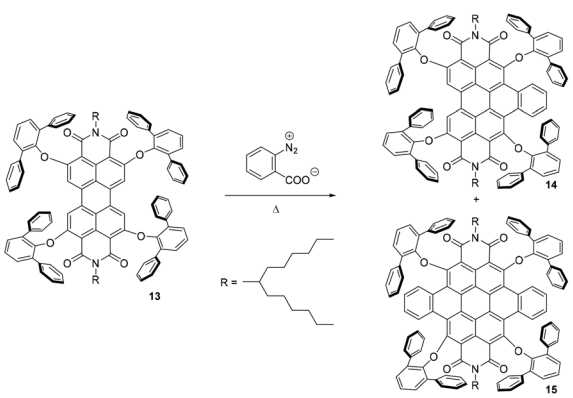

Scheme 4 Synthesis of **14** and **15**.

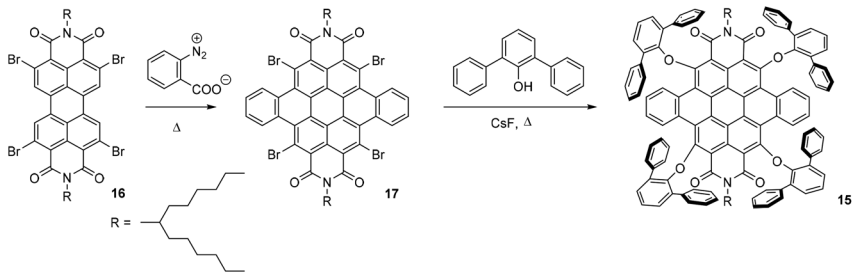

Scheme 5 Indirect synthesis of **15**.

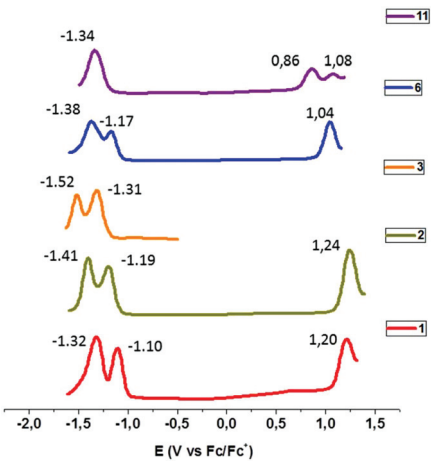

Fig. 5 DPV data for compounds **1–3**, **6** and **11** (redox potentials were measured in CH_2Cl_2 with 0.1 M $TBAPF_6$ *vs.* Fc/Fc^+).

(HOMO) and lowest-unoccupied (LUMO) molecular orbitals. The introduction of additional benzannulated rings hinders both the oxidation and the reduction to such an extent that we were not able to oxidize **3** in methylene chloride. The effect of the core extension is more pronounced in the reduction processes, with cathodic shifts of 90 and 210 mV for the first reduction potential of **2** and **3**, respectively, thus indicating a reduced electron-accepting ability of these compounds compared to **1**. Fussion of a new benzene ring on compound **2** changes the tendency, and the resulting compound, *i.e.* **6**, has lower oxidation and reduction potentials than **2**. Indeed, the oxidation of **6** is 200 mV easier than the oxidation of **1** (Fig. 5 and Table 5). The electron-rich nature of pyrrole compared with benzene brings about an additional cathodic shift of the oxidation potential, and makes the oxidation of the pyrrolo-fused compound **11** 180 mV easier than in the case of **6** (Fig. 5).

Table 5 Redox potentials measured by DPV (CH_2Cl_2 solution containing 0.1 M $TBAPF_6$ as the supporting electrolyte and Fc/Fc^+ as the internal standard) and estimated energies of the frontier orbitals

Compound	$E_{red,2}$ (V)	$E_{red,1}$ (V)	$E_{ox,1}$ (V)	$E_{ox,2}$ (V)	HOMO[a] (eV)	LUMO[a] (eV)
1	−1.32	−1.10	1.20		−6.00	−3.70
2	−1.41	−1.19	1.24		−6.04	−3.61
3	−1.52	−1.31			−6.00[b]	−3.49
6	−1.38	−1.17	1.04		−5.84	−3.63
11		−1.34	0.86	1.08	−5.66	−3.47

[a] Calculated according to the equations: $E_{LUMO} = -E_{red,1} - 4.8$ and $E_{HOMO} = -E_{ox,1} - 4.8$. [b] $E_{HOMO} = E_{LUMO} + 1224/\lambda_{00}$, where λ_{00} is the wavelength at the intersection of the absorption spectrum with the normalized emission spectrum.

Absorption and emission spectra

Fig. 6a shows the UV-vis spectra of compounds **1–3** in dichloromethane. The extension of conjugation causes a gradual hypsochromic shift of the absorption spectrum and a decrease of the molar absorption coefficient. The change is slightly more pronounced when passing from **1** (524 nm) to **2** (505 nm) than when we consider the transformation of **2** to **3** (490 nm). However, it is interesting to note that **3** represents a kind of minimum in the λ_{max} values, as the absorption of **6** (with a benzene ring fused on the structure of **2**) moves batho-

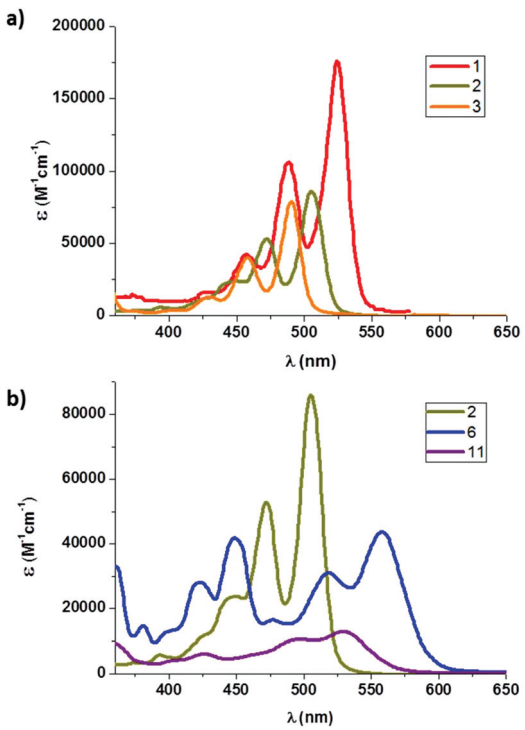

Fig. 6 UV-vis spectra recorded for **1–3** (a) and **2**, **6** and **11** (b) in CH_2Cl_2.

chromically to 558 nm, thus recovering the usual red shift observed with core expansion (Fig. 6b). It is to note that the extinction coefficient of **6** drops dramatically compared to **2**. When compared to **6** (λ_{max} = 558 nm), the pyrrolo-fused core-extended derivative **11** exhibits a lower bathochromic shift in the lowest-energy absorption band (533 nm) with respect to **2** (505 nm), even though pyrrole is an electron-rich aromatic ring (Fig. 6b). This is probably due to the nonlinear way of fusion of the pyrrole ring to the NPDI core. The extinction coefficient recorded for **11** is even lower than that of **6**.

The emission spectra of compounds **1–3**, **6** and **11** are collected in Fig. 7. As expected, emission maxima for these compounds show the same trends discussed above for the absorption spectra. The emission maximum shifts to the blue upon extending the PDI core from **1** to **2** and **3**, shifts to the red in passing from **2** to **6** and goes back to the blue for **11**. The presence of sequential emission peaks decreasing in intensity upon decreasing in energy suggests a vibronic structure that is confirmed below with the help of theoretical calculations.

The fluorescence emission is partially quenched for the halogenated systems **9** and **12**, due to the electron lone pairs present in the halogen atoms. The effect is more pronounced for compound **5** (Φ_f = 0.50), which bears iodine atoms like **4** (Φ_f = 1.00), and for **6** (Φ_f = 0.15) with no halogen atom. For these compounds the higher quenching should be therefore associated to their higher tendency to aggregate owing to their largely extended π-conjugated structure. Finally, the quenching is almost complete in **11**, which contains a fused electron-rich nitrogenous ring (Table 6).

Table 6 Absorption and emission maxima and fluorescence quantum yields (Φ_f)

Compound	UV-vis λ_{max} (nm)	Emission λ_{max} (nm)	Φ_f
1	458, 488, 524	532, 575	1.00
2	472, 505	516, 554	1.00
3	458, 490	500, 534	1.00
4	441, 469, 503	515, 551	1.00
5	433, 462, 493	531	0.50
6	422, 449, 471, 518, 558	597	0.15
7	496, 530, 573 (ref. 8*e*)	584 (ref. 8*e*)	
8	437, 449, 467, 499	510, 546	1.00
9	422, 448, 468, 506	507, 543	0.80
11	429, 501, 533	534, 578	0.04
12	402, 426, 450, 477, 507	519, 556	0.84

Theoretical calculations

To give insight into the effect that the transversal π-extension of the PDI core has on the electronic and optical properties of core-expanded PDI derivatives, we performed a comprehensive theoretical analysis under the density functional theory (DFT) framework. The study considers the series of perylenediimides with asymmetric (**a**) and symmetric (**s**) core expansion constituted by compounds **1**, **aCDI**, **sCDI**, **2–4**, **6–9** and **11** (Fig. S57‡). Methyl groups were introduced in the imido end positions as axial *N*-substituents. Note that **aCDI** is included in the series for the sake of comparison although its synthesis has not been reported so far.

The minimum-energy geometries computed at the B3LYP/6-31G* level of theory for the list of PDIs are displayed in Fig. S57 in the ESI.‡ All the compounds show planar conjugated cores along with coplanar diimide terminal groups, and with alternating single and double C–C bonds in the range of 1.39–1.46 Å. Although no symmetry constraint was imposed, the symmetric core-expanded PDIs **1**, **sCDI**, **3** and **7** show D_{2h} molecular point group symmetry (excluding the terminal methyl moieties). Otherwise, asymmetric core-expanded **aCDI**, **2** and **6** present C_{2v} point group symmetry. Substituted PDIs **4**, **8** and **9** show C_s molecular symmetry, and **11** is C_1 due to a slight out-of-plane distortion of the pyrrole moiety with respect to the PDI core to avoid H···H close contacts (Fig. S57‡).

A first approach to transversal core extension (level 1 in Fig. 8) is through insertion of a C=C double bond in one (asymmetric **aCDI**) or the two sides (symmetric **sCDI**) of the PDI system. Instead of narrowing the HOMO–LUMO gap (E_{H-L}), this level-1 core extension increases E_{H-L} from 2.54 eV in **1** to 2.94 eV in **aCDI**, and to 3.18 eV in **sCDI** (Fig. S58‡). Generation of benzene-like HOMOs (*i.e.* stabilization of the HOMO) and a larger amount of antibonding interactions in the LUMO (*i.e.* destabilization of the LUMO) going from **1** to **aCDI** and to **sCDI** (Fig. S58‡) explains this trend and the hypso-

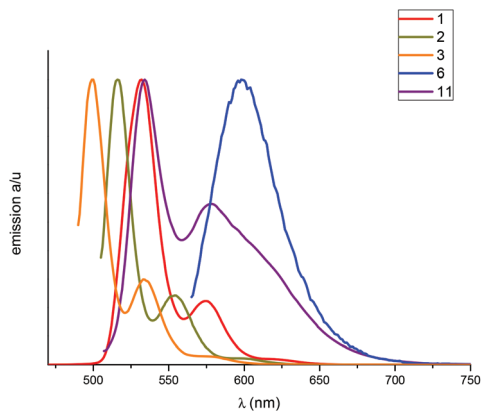

Fig. 7 Normalized emission spectra of **1**, **2**, **3**, **6** and **11** in CH_2Cl_2.

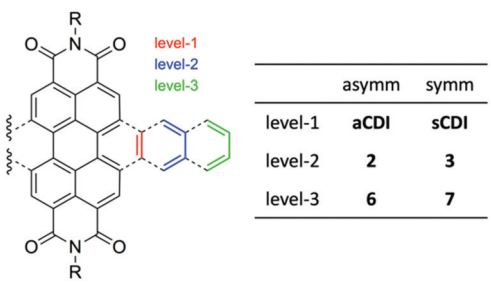

Fig. 8 Levels of core expansion in symmetric and asymmetric transversally core-extended PDIs.

chromic shift of the lowest electronic transition in the absorption spectrum, as recently reported.[7]

Further transversal core extension cannot occur by incorporating additional C=C fragments but four carbon atoms in the form of C=C–C=C fragments are required (Fig. 8). In this level-2 core extension, asymmetric NPDI **2** and symmetric DBCDI **3** derivatives are obtained. Incorporation of entire benzene rings from **1** to **2** and to **3** leads to a hypsochromic shift of the lowest-lying absorption band, similarly to that found for **sCDI**. Theoretical calculations indicate that the HOMO energies are barely affected by this π-extension, as only weak additional antibonding interactions are formed (Fig. 9 and S58‡). In contrast, the extra peripheral benzene rings contribute with new destabilizing antibonding interactions in the LUMO, leading to a significant increase of the LUMO energy in going from **1** (−3.46 eV) to **2** (−3.28 eV) and to **3** (−3.13 eV). This is in line with the poorer electron-accepting ability obtained in the electrochemical data moving from **1** to **2**, and to **3** (Fig. 5 and Table 5), and with the theoretical electron affinity (EA) trends: EA values of 2.34, 2.20 and 2.10 eV are calculated for **1**, **2** and **3**, respectively (Table S1‡). As a result, a systematic increase of the HOMO–LUMO gap is predicted upon level-2 core extension in going from **1** (2.54 eV) to **2** (2.68 eV) and to **3** (2.80 eV).

Time-dependent DFT calculations show that the lowest-lying singlet excited state S_1 of PDIs is described by a mono-electronic excitation from the HOMO to the LUMO (Table 7). The S_1 state is calculated at 2.44 eV (507 nm) for **1**, and hypsochromically shifts to 2.49 eV (498 nm) in **2** and to 2.54 eV (488 nm) in **3**, in accordance with the HOMO–LUMO gap

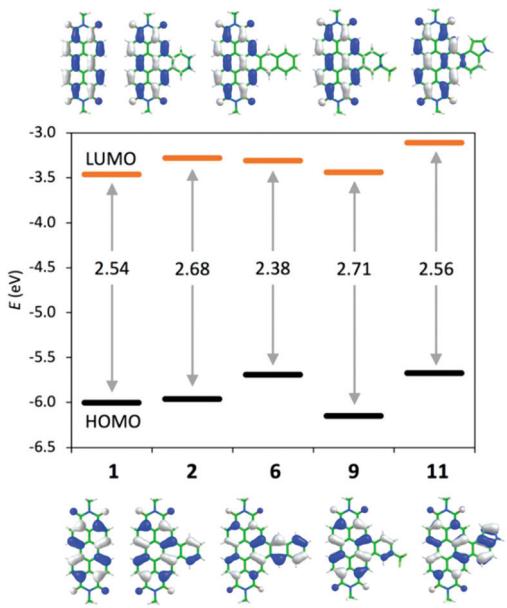

Fig. 9 Energy diagram of the highest-occupied (HOMO) and lowest-unoccupied (LUMO) molecular orbitals of PDIs with asymmetric core expansion. The topologies of the HOMO (bottom) and LUMO (top) are displayed.

Table 7 Vertical excitation energy (*E*, in eV and nm), oscillator strength (*f*) and HOMO → LUMO contribution (in %) calculated for the $S_0 \rightarrow S_1$ electronic transition at the B3LYP/6-31G* level of theory

Compound	*E* (eV)	*E* (nm)	*f*	H → L (%)
1	2.44	507	0.668	100
2	2.49	498	0.467	98
3	2.54	488	0.335	88
4	2.49	498	0.443	98
6	2.09	594	0.187	96
7	2.07	599	0.183	97
8	2.51	495	0.470	95
9	2.53	490	0.493	98
11	2.26	549	0.210	98

trends discussed above and in very good agreement with the UV-vis absorption spectra (Fig. 6). Upon increasing the π-conjugation in **2** and **3**, the HOMO spreads transversally whereas the topology of the LUMO is preserved, leading to a reduction of the HOMO–LUMO overlap (Fig. 9 and S58‡). As a result, the oscillator strength (*f*) of the $S_0 \rightarrow S_1$ excitation in the core-extended derivatives is predicted to decrease from *f* = 0.668 in **1** to 0.467 in **2** and to 0.335 in **3**, nicely reproducing the drop in intensity experimentally observed for the absorption band (Fig. 6a).

Theoretical calculations indicate that further increase of the transversal core extension (level-3, Fig. 8) from **2** or **3** leads to a reduction of the HOMO–LUMO gap, with E_{H-L} values of 2.38 eV in **6** and 2.37 eV in **7**. This stems from a destabilization of the HOMO from **2** to **6** (+0.27 eV), and from **3** to **7** (+0.38 eV), as anticipated by increasing the π-conjugation. These results nicely correlate with the significant lower oxidation potential recorded for **6** and **7** compared to **2** and **3**, respectively (Table 5), and with the theoretical values calculated for the first ionization potential (IP): 6.77 and 7.10 eV for **6** and **2**, and 6.52 and 7.00 eV for **7** and **3**, respectively (Table S1‡). The lowest-lying S_1 state is predicted with the expected bathochromic shift upon level-3 core extension, with excitation energies of 2.09 eV and 2.07 eV for **6** and **7**, respectively, in agreement with the experimental UV-Vis data (Table 6). The intensity of S_1 for the core-extended derivatives **6** and **7** is expected to be smaller due to the reduced HOMO–LUMO overlap, and *f* is indeed computed to be smaller than 0.2.

The effect of introducing electron-withdrawing (fluorine **9**, iodine **4**, and carboxylic acid **8**) and electron-donor (pyrrole, **11**) groups on the electronic and optical features of PDIs was also analysed. We consider here the series of asymmetric analogues of **2**, but trends can be extrapolated to the other related core-extended derivatives. Insertion of electron-withdrawing groups in the transversal region of the PDI structure leads to a stabilization of the frontier molecular orbitals: from −5.93 eV to −6.15 eV in the HOMO and from −3.13 eV to −3.44 eV in the LUMO in going from **2** to **9**, respectively, with intermediate values for **4** and **8** (Fig. S58‡). As a result, the HOMO–LUMO gap slightly increases from 2.68 eV in **2** to 2.71 eV in **9**. Conversely, the fusion of an electron-rich pyrrole ring from **2** to **11** results in a destabilization of both HOMO (+0.29 eV) and

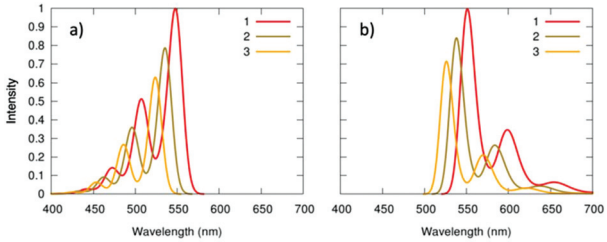

Fig. 10 Vibrationally-resolved theoretical absorption (a) and emission (b) spectra calculated for the lowest-lying singlet excitation ($S_0 \rightarrow S_1$) in PDI derivatives **1–3**. Intensities are normalized to the highest peak of compound **1**.

LUMO (+0.17 eV) orbitals. Theoretical calculations suggest a larger destabilization in the case of the HOMO due to the direct participation of the pyrrole moiety into the π-extension of the molecular orbital (Fig. 9). This trend explains the lower oxidation potential recorded for the pyrrolo-fused compound compared to **2** (Fig. 5), which nicely agrees with the smaller theoretical IP of 6.77 eV calculated for **11** compared to **2** (7.10 eV, Table S1‡). The HOMO–LUMO gap is therefore reduced from 2.68 eV in **2** to 2.56 eV in **11**. The lowest-lying S_1 state for **11** is thus computed at larger wavelengths (2.26 eV; 549 nm) and with lower intensity ($f = 0.210$) compared to unsubstituted **2**, in good accord with the experimental UV-vis results (Fig. 6b).

Finally, the vibrational resolution of the theoretical absorption spectra corresponding to the highly-intense, lowest-lying $S_0 \rightarrow S_1$ excitation was analysed for compounds **1–3** (see the Experimental section for details). The simulated absorption spectrum for **1** (Fig. 10a) indicates that the lowest absorption band presents a well-resolved vibrational structure, leading to a series of peaks at 550, 505, 470 and 440 (shoulder) nm, which nicely agree with the experimental features found at 525, 480, 455 and 425 nm (Fig. 6a). This suggests that the UV-vis absorption spectrum of **1** is mainly governed by the vibronic structure of the intense $S_0 \rightarrow S_1$ excitation. Increasing the π-core from **1** to **2** and to **3** results in a displacement of the absorption features to higher energies, with a total blue shift of *ca.* 25 nm to be compared with the experimental blue shift of 30 nm, along with a decrease in the absorption intensity as discussed above. Similarly, the simulated emission spectrum of **1** (Fig. 10b) shows a well-resolved vibronic structure with peaks at 550, 600 and 650 nm, which can be assigned to the experimental features observed at 530, 575 and 625 (shoulder) nm. Moving from **1** to π-extended **3** leads to a *ca.* 25 nm blue shift of the emission features, in line with the theoretical absorption evolution and in good accord with the experimental findings (Fig. 7).

Experimental

Materials and methods

Solvents and reagents were obtained from commercial sources and used as received. Column chromatography: SiO_2 (40–63 μm) TLC plates coated with SiO_2 60F254 were visualized by UV light. NMR spectra were recorded at 25 °C using a Bruker AC300 spectrometer. The solvents for spectroscopic studies were of spectroscopic grade and used as received. UV/vis spectra were measured with a Helios Gamma spectrophotometer. IR spectra were recorded with a Nicolet Impact 400D spectrophotometer. High resolution mass spectra were obtained from a Bruker Reflex II matrix-assisted laser desorption/ionization time of flight (MALDI-TOF) using dithranol as matrix. Fluorescence emission spectra were recorded on a Perkin Elmer LS55 spectrofluorometer and fluorescence quantum yields were calculated using PDI **1** as the standard ($\Phi_f = 1$).[1b]

Synthesis method A. Anthranilic acid (10 mmol) and trichloroacetic acid (0.33 mmol) were dissolved in dry THF (20 mL). This solution was cooled at 0 °C and isopentyl nitrite (0.43 mmol) was dropped over 30 min. The mixture was stirred 30 min at 0 °C and 2 h at room temperature. Then, the precipitate was filtered and washed with cold dry THF, and the solid was mixed with the PDI (0.2 mmol) and THF (10 mL). The reaction was refluxed 24 h and, after cooling, it was partitioned with dichloromethane and water. The organic layer was dried over anhydrous sodium sulfate, filtered and evaporated. Purification was carried out by silica gel column chromatography using the solvent specified for each compound.

Synthesis method B. Anthranilic acid (10 mmol) and trichloroacetic acid (0.33 mmol) were dissolved in dry THF (20 mL). This solution was cooled at 0 °C and isopentyl nitrite (0.43 mmol) was dropped over 30 min. The mixture was stirred 30 min at 0 °C and 2 h at room temperature. Then, the precipitate was filtered and washed with cold dry THF, and the solid was mixed with the PDI (0.2 mmol) and THF (5 mL). The reaction was refluxed 36 h and, after cooling, it was partitioned with dichloromethane and water. The organic layer was dried over anhydrous sodium sulfate, filtered and evaporated. Purification was carried out by silica gel column chromatography using the solvent specified for each compound.

Synthesis method C. 2-(Trimethylsilyl)phenyl trifluoromethanesulfonate (0.5 mmol), PDI (0.1 mmol), and CsF (1 mmol) were dissolved in a mixture of toluene : acetonitrile 1 : 1 (2 mL) and heated at 80 °C under argon atmosphere for 24 h. After cooling, it was partitioned with dichloromethane and water. The organic layer was dried over anhydrous sodium sulfate, filtered and evaporated. Purification was carried out by silica gel column chromatography using the solvent specified for each compound.

Synthesis method D. 2-(Trimethylsilyl)phenyl trifluoromethanesulfonate (1 mmol), PDI (0.1 mmol), and CsF (1.2 mmol) were dissolved in a mixture of toluene : acetonitrile 1 : 1 (1 mL) and heated at 80 °C under argon atmosphere for 36 h. After cooling, it was partitioned with dichloromethane and water. The organic layer was dried over anhydrous sodium sulfate, filtered and evaporated. Purification was carried out by silica gel column chromatography using the solvent specified for each compound.

(2) Yield: 70%. Orange solid. Purification was carried out using chloroform : toluene 3 : 1 as eluent. ^{1}H-RMN ($CDCl_3$) δ 0.91 (t, 12H), 1.37–1.51 (br, 32H), 2.13 (m, 4H), 2.37 (m, 4H),

5.29 (m, 2H), 7.85 (dd, 2H), 8.43 (br, 4H), 8.57 (d, 2H), 9.01 ppm (s, 2H). ^{13}C-RMN ($CDCl_3$) δ 164.13, 163.37, 132.09, 128.39, 127.82, 126.64, 126.01, 123.19, 122.80, 122.53, 121.84, 54.92, 32.51, 31.90, 29.40, 27.34, 22.71, 14.11 ppm. HRMS MALDI-TOF *m*/*z*: [M^+] calcd for $C_{56}H_{64}N_2O_4$: 828.493, found: 828.496. IR (KBr): 2962, 2925, 2851, 1707, 1658, 1597, 1409, 1352, 1319, 1245, 804, 747 cm^{-1}. UV-vis (CH_2Cl_2), λ_{max}/nm (log ε): 472 (4.7), 505 (4.9). Φ_f = 1.00.

(3) Yield: 80%. Orange solid. Purification was carried out using chloroform : toluene 3 : 1 as eluent. ^{1}H-RMN ($CDCl_3$) δ 0.91 (t, 12H), 1.25–1.58 (m, 32H), 2.26 (m, 4H), 2.54 (m, 4H), 5.41 (m, 2H), 8.18 (d, 4H), 8.92 (m, 4H), 9.54 ppm (s, 4H). ^{13}C-RMN ($CDCl_3$) δ 128.87, 128.69, 127.30, 124.06, 123.07, 122.53, 121.13, 55.17, 32.64, 31.92, 29.69, 29.47, 27.39, 22.73, 14.12 ppm. HRMS MALDI-TOF *m*/*z*: [M^+] calcd for $C_{62}H_{66}N_2O_4$: 902.5023, found: 902.5063. IR (KBr): 2926, 2850, 1695, 1654, 1607, 1438, 1316, 1246, 744 cm^{-1}. UV-vis (CH_2Cl_2), λ_{max}/nm (log ε): 458 (4.6), 490 (4.9). Φ_f = 1.00.

(4) Yield: 75%. Yellow solid. Purification was carried out using chloroform : toluene 3 : 1 as eluent. ^{1}H-RMN ($CDCl_3$) δ 0.84 (t, 12H), 1.28–1.41 (br, 32H), 2.02 (m, 4H), 2.39 (m, 4H), 5.31 (m, 2H), 8.28 (d, 1H), 8.72 (d, 1H), 9.00 (m, 4H), 9.38 (s, 1H), 9.72 ppm (d, 2H). ^{13}C-RMN ($CDCl_3$) δ 137.34, 133.01, 130.34, 127.89, 127.69, 127.20, 127.14, 126.57, 125.22, 124.52, 124.18, 124.15, 124.09, 122.99, 95.70, 55.11, 32.53, 31.82, 29.30, 27.12, 22.62, 14.05 ppm. HRMS MALDI-TOF *m*/*z*: [M^+] calcd for $C_{56}H_{63}N_2O_4I$: 954.3827, found: 954.3861. IR (KBr): 2956, 2926, 2856, 1707, 1649, 1608, 1474, 1415, 1357, 1316, 1246, 1170, 808, 744 cm^{-1}. UV-vis (CH_2Cl_2), λ_{max}/nm (log ε): 441 (4.4), 469 (4.8), 503 (4.9). Φ_f = 1.00.

(5) Yield: 56%. Orange solid. Purification was carried out using chloroform : toluene 3 : 1 as eluent. ^{1}H-RMN ($CDCl_3$) δ 0.86 (t, 12H), 1.25–1.33 (br, 22H), 1.52 (m, 10H), 2.19 (m, 4H), 2.54 (m, 4H), 5.46 (m, 2H), 8.48 (d, 2H), 8.96 (d, 2H), 9.56 (m, 2H), 10.05 ppm (m, 4H). ^{13}C-RMN ($CDCl_3$) δ 158.44, 157.87, 146.94, 140.81, 139.19, 138.91, 138.53, 132.16, 131.05, 129.57, 124.00, 121.97, 117.46, 114.44, 68.82, 68.70, 55.84, 37.37, 32.99, 32.14, 32.09, 31.71, 30.51, 30.39, 30.28, 30.16, 29.92, 29.59, 29.55, 28.19, 27.83, 27.55, 27.32, 27.08, 26.16, 22.91, 20.05, 14.36 ppm. HRMS MALDI-TOF *m*/*z*: [M^+] calcd for $C_{62}H_{64}N_2O_4I_2$: 1154.2949, found: 1154.2967. IR (KBr): 2954, 2913, 2844, 1741, 1709, 1654, 1590, 1466, 1379, 1310, 1237, 1182, 1086, 811, 752 cm^{-1}. UV-vis (CH_2Cl_2), λ_{max}/nm (log ε): 433 (3.6), 462 (4.0), 493 (4.2). Φ_f = 0.50.

(6) Yield: 38%. Orange solid. Purification was carried out using toluene as eluent. ^{1}H-RMN ($CDCl_3$) δ 0.86 (t, 12H), 1.28 (br, 32H), 2.02 (m, 4H), 2.42 (m, 4H), 5.34 (m, 2H), 7.83 (d, 2H), 8.27 (d, 2H), 8.98 (m, 4H), 9.50 (s, 2H), 9.8 ppm (s, 2H). ^{13}C-RMN ($CDCl_3$) δ 164.25, 163.63, 133.11, 132.05, 128.26, 127.51, 127.06, 126.19, 124.34, 124.28, 124.22, 122.83, 122.49, 55.05, 32.56, 31.91, 31.89, 29.68, 29.39, 27.24, 22.67, 14.08 ppm. HRMS MALDI-TOF *m*/*z*: [M^+] calcd for $C_{60}H_{66}N_2O_4$: 878.5017, found: 878.5088. IR (KBr): 2959, 2923, 2836, 1695, 1649, 1590, 1466, 1416, 1329, 1306, 1246, 862, 811, 743 cm^{-1}. UV-vis (CH_2Cl_2), λ_{max}/nm (log ε): 422 (4.1), 449 (4.3), 477 (3.9), 518 (4.2), 558 (4.3). Φ_f = 0.15.

(8) Yield: 28%. Orange solid. Purification was carried out using dichloromethane : methanol 5 : 0.1 as eluent. ^{1}H-RMN ($CDCl_3$) δ 0.90 (m, 12H), 1.26 (br, 32H), 2.14 (br, 4H), 2.56 (br, 4H), 3.60 (m, 1H), 5.24 (br, 1H), 5.46 (br, 1H), 8.92 (m, 6H), 9.60 (br, 2H), 9.77 ppm (br, 1H). ^{13}C-RMN ($CDCl_3$) δ 171.41, 163.58, 159.06, 133.07, 132.31, 131.52, 130.50, 129.43, 126.90, 124.63, 124.03, 123.51, 122.68, 122.47, 120.77, 115.06, 114.15, 72.81, 70.36, 69.36, 67.94, 67.16, 55.28, 38.54, 37.87, 32.64, 31.92, 31.88, 29.68, 29.44, 29.31, 27.31, 26.29, 26.10, 25.49, 25.11, 23.83, 22.71, 22.63, 14.12, 14.09 ppm. HRMS MALDI-TOF *m*/*z*: [M^+] calcd for $C_{57}H_{64}N_2O_6$: 872.4764, found: 872.4650. IR (KBr): 3416, 2958, 2913, 2844, 1708, 1654, 1593, 1446, 1417, 1319, 1254, 1205, 1160, 1099, 813, 747 cm^{-1}. UV-vis (CH_2Cl_2), λ_{max}/nm (log ε): 437 (3.9), 449 (4.0), 467 (4.3), 499 (4.5). Φ_f = 1.00.

(9) Yield: 22%. Yellow solid. Purification was carried out using toluene as eluent. ^{1}H-RMN ($CDCl_3$) δ 0.81 (t, 12H), 1.26 (br, 32H), 1.98 (m, 4H), 2.39 (m, 4H), 5.34 (m, 2H), 8.33 (d, 1H), 9.08 (s, 2H), 9.24 (d, 2H), 9.41 (d, 1H), 9.57 (s, 1H), 10.17 ppm (s, 2H). ^{13}C-RMN ($CDCl_3$) δ 165.57, 161.64, 134.20, 134.11, 133.83, 130.22, 129.12, 128.44, 127.95, 127.82, 127.19, 127.14, 125.70, 125.65, 124.87, 114.90, 67.89, 65.45, 32.81, 32.02, 29.95, 29.50, 27.34, 27.32, 26.18, 26.11, 25.75, 22.87, 14.34 ppm. HRMS MALDI-TOF *m*/*z*: [M^+] calcd for $C_{57}H_{63}N_2O_4F_3$: 896.4734, found: 896.4726. IR (KBr): 2927, 2862, 1703, 1666, 1591, 1465, 1423, 1320, 1245, 1166, 1128, 1067, 834, 810 cm^{-1}. UV-vis (CH_2Cl_2), λ_{max}/nm (log ε): 422 (3.9), 448 (4.3), 468 (4.6), 506 (4.9). Φ_f = 0.80.

(11) Yield: 64%. Yellow solid. Purification was carried out using dichloromethane as eluent. ^{1}H-RMN ($CDCl_3$) δ 0.87 (t, 12H), 1.35–1.50 (br, 32H), 2.15 (m, 4H), 2.40 (m, 4H), 5.32 (m, 2H), 7.56 (d, 2H), 7.91 (d, 1H), 8.38 (d, 1H), 8.50–8.69 (m, 4H), 9.19 (s, 1H), 9.32 (s, 1H), 9.89 ppm (s, 1H). ^{13}C-RMN ($CDCl_3$) δ 135.05, 132.52, 132.13, 127.97, 127.68, 125.83, 125.73, 124.88, 124.33, 124.22, 123.05, 121.83, 121.40, 117.59, 114.65, 106.61, 54.85, 32.58, 31.91, 29.44, 27.34, 22.69, 14.10 ppm. HRMS MALDI-TOF *m*/*z*: [M^+] calcd for $C_{58}H_{65}N_2O_4$: 867.4969, found: 867.4934. IR (KBr): 3306, 2956, 2926, 2845, 1701, 1654, 1590, 1415, 1357, 1310, 1246, 1170, 1094, 808, 744, 715 cm^{-1}. UV-vis (CH_2Cl_2), λ_{max}/nm (log ε): 429 (3.7), 501 (4.0), 533 (4.1). Φ_f = 0.04.

(12) Yield: 43%. Yellow solid. Purification was carried out using toluene as eluent. ^{1}H-RMN ($CDCl_3$) δ 0.84 (t, 12H), 1.25 (br, 32H), 2.03 (m, 4H), 2.36 (m, 4H), 5.31 (m, 2H), 7.91 (m, 2H), 8.11 (d, 1H), 9.04 (m, 4H), 9.82 (s, 1H), 11.09 ppm (s, 1H). ^{13}C-RMN ($CDCl_3$) δ 133.37, 132.81, 132.41, 131.63, 128.07, 127.91, 127.50, 127.13, 126.83, 126.34, 125.75, 124.60, 123.90, 123.84, 123.62, 123.08, 122.95, 122.77, 32.50, 31.81, 29.69, 29.30, 27.14, 27.10, 22.62, 14.05 ppm. HRMS MALDI-TOF *m*/*z*: [M^+] calcd for $C_{56}H_{63}N_2O_4Cl$: 862.4476, found: 862.4407. IR (KBr): 2961, 2927, 2851, 1702, 1656, 1601, 1419, 1348, 1310, 1246, 1175, 1082, 807, 723 cm^{-1}. UV-vis (CH_2Cl_2), λ_{max}/nm (log ε): 402 (3.7), 426 (3.9), 450 (4.2), 477 (4.5), 507 (4.7). Φ_f = 0.84.

(14) Yield: 61%. Orange solid. Purification was carried out using dichloromethane : hexane 1 : 1 as eluent. ^{1}H-RMN (50 °C, $CDCl_3$) δ 0.92 (t, 12H), 1.34 (br, 32H), 1.72 (m, 2H), 1.89

(m, 4H), 2.23 (m, 2H), 5.15 (m, 2H), 6.37 (br, 10H), 6.71 (br, 2H), 7.10 (m, 30H), 7.47 (br, 2H), 7.68 (m, 12H), 9.20 ppm (br, 2H). ^{13}C-RMN ($CDCl_3$) δ 162.06, 157.67, 152.46, 152.32, 146.85, 146.51, 145.33, 140.89, 138.65, 137.38, 137.32, 137.26, 135.78, 135.72, 133.54, 132.11, 131.35, 131.17, 130.94, 130.14, 130.13, 129.46, 129.25, 128.81, 128.54, 127.97, 127.85, 127.57, 127.26, 126.95, 126.87, 126.46, 125.85, 125.79, 124.64, 124.26, 123.70, 123.28, 122.44, 121.69, 115.09, 107.54, 53.93, 32.42, 31.97, 29.45, 27.14, 22.80, 14.18 ppm. HRMS MALDI-TOF *m*/*z*: [M + H$^+$] calcd for $C_{128}H_{112}N_2O_8$: 1805.8491, found: 1805.8413. IR (KBr): 3064, 3023, 2950, 2913, 2844, 1695, 1645, 1590, 1567, 1503, 1462, 1411, 1347, 1288, 1223, 1182, 907, 756, 701 cm^{-1}. UV-vis (CH_2Cl_2), λ_{max}/nm (log ε): 494 (4.3), 525 (4.4). Φ_f = 0.17.

(15) Yield: 89%. Orange solid. Purification was carried out using dichloromethane : hexane 1 : 1 as eluent. ^{1}H-RMN (50 °C, $CDCl_3$) δ 0.93 (t, 12H), 1.33 (m, 32H), 1.69 (m, 4H), 4.63 (m, 2H), 6.50 (m, 8H), 6.66 (m, 14H), 7.17 (m, 30H), 7.83 (m, 4H), 9.73 ppm (m, 4H). ^{13}C-RMN ($CDCl_3$) δ 158.84, 152.26, 138.81, 132.67, 131.48, 129.11, 128.85, 127.98, 126.97, 126.16, 125.94, 124.80, 123.94, 123.15, 122.75, 32.83, 32.01, 29.69, 29.47, 27.63, 22.86, 14.19 ppm. HRMS MALDI-TOF *m*/*z*: [M + H$^+$] calcd for $C_{134}H_{114}N_2O_8$: 1879.8547 found: 1879.8589. IR (KBr): 3065, 3023, 2959, 2923, 2849, 1700, 1659, 1576, 1494, 1462, 1411, 1379, 1343, 1311, 1219, 1169, 912, 752, 697 cm^{-1}. UV-vis (CH_2Cl_2), λ_{max}/nm (log ε): 458 (3.7), 489 (4.0), 522 (4.2), 551 (4.1). Φ_f = 0.24.

(17) Yield: 86%. Orange solid. Purification was carried out using dichloromethane : hexane 3 : 1 as eluent. ^{1}H-RMN ($CDCl_3$) δ 0.85 (br, 12H), 1.31 (br, 32H), 2.04 (m, 4H), 2.44 (m, 4H), 5.36 (m, 2H), 7.85 (m, 4H), 9.70 ppm (m, 4H). ^{13}C-RMN ($CDCl_3$) δ 142.84, 141.24, 131.30, 130.96, 130.59, 128.59, 128.28, 127.28, 127.15, 126.21, 125.86, 124.12, 121.11, 119.82, 61.49, 56.45, 32.52, 32.27, 31.80, 29.22, 29.13, 27.03, 26.93, 22.60, 14.11, 14.08 ppm. HRMS MALDI-TOF *m*/*z*: [M + H$^+$] calcd for $C_{62}H_{62}N_2O_4Br_4$: 1214.1443 found: 1214.1910. IR (KBr): 2950, 2938, 2845, 1742, 1707, 1660, 1590, 1310, 1246, 1176, 814 cm^{-1}. UV-vis (CH_2Cl_2), λ_{max}/nm (log ε): 494 (4.3), 508 (4.3), 530 (4.4). Φ_f = 1.00.

Theoretical calculations. Density functional theory (DFT) calculations were performed by using the Gaussian 09.D01 suite of programs.[17] Minimum-energy geometries for the perylenediimide derivatives with variable transversal π-extension were obtained using the hybrid Becke3–Lee–Yang–Parr (B3LYP) functional[18] and the Pople's double-zeta 6-31G* basis set.[19] Frequency calculations were performed to confirm the minimum nature of the structures. Molecular orbitals were represented using an isovalue contour of ±0.03 a.u. by means of the Chemcraft software.[20] TD-DFT calculations were performed at the B3LYP/6-31G* level for the lowest-lying 30 singlet excited states in gas phase.[21] Simulated absorption and emission spectra were obtained by using the Franck–Condon approximation for the lowest-lying singlet excited state S_1. The half-width at half-maximum (HWHM) for the vibronic Gaussian-convoluted spectra was set to 300 cm^{-1} (0.04 eV). Redox properties (ionization potential, electron affinity and reorganization energies) were obtained for the family of perylenediimide derivatives by calculating the singly-charged cation and anion species. Minimum-energy geometries of the cations and anions were obtained by using the spin-unrestricted UB3LYP/6-31G* approach.

Conclusions

In summary, we have developed a simple and efficient synthetic protocol, based on the Diels–Alder reaction of PDIs with benzynes, to expand the aromatic π system of the formers. This methodology further allows the use of functionalized benzynes and PDIs in order to obtain new and interesting derivatives. Theoretical calculations performed at the DFT level are able to fully rationalize the unexpected changes observed for the electronic, optical and redox properties of the PDIs upon transversal core-extension up to three different level. The level-2 π-expansion of the PDI core leading to asymmetric NPDI **2** and symmetric DBCDI **3** implies a reduction of the acceptor ability (more negative reduction potentials and smaller electron affinities) and a hypsochromic shift of the absorption and emission band. In contrast, the level-3 π-expansion of the PDI core to compounds **6** and **7** leads to a bathochromic shift of both absorption and emission. These changes have been rationalized by analysing the energies and topologies of the frontier molecular orbitals and the overlap between them. The results presented in this work are expected to guide the design and discovery of novel PDIs with target properties for advanced materials applications.

Conflicts of interest

There are no conflicts to declare.

Acknowledgements

We gratefully acknowledge the financial support provided by the Spanish Ministry of Economy and Competitiveness MINECO (CTQ2015-71154-P, CTQ2016-77039-R, and Unidad de Excelencia María de Maeztu MDM-2015-0538), the Generalitat Valenciana (PROMETEO/2016/135) and European Feder funds (CTQ2015-71154-P and CTQ2016-77039-R). J. C. also acknowledges the Generalitat Valenciana for a VALi+D post-doctoral fellowship (APOSTD/2017/081).

Notes and references

1 (*a*) H. Langhals, *Heterocycles*, 1995, **40**, 477–500; (*b*) F. Würthner, *Chem. Commun.*, 2004, 1564–1579; (*c*) H. Langhals, *Helv. Chim. Acta*, 2005, **88**, 1309–1343; (*d*) F. Würthner, *Pure Appl. Chem.*, 2006, **78**, 2341–2349; (*e*) A. Herrmann and K. Müllen, *Chem. Lett.*, 2006, **35**, 978–985; (*f*) F. Würthner, C. R. Saha-Möller, B. Fimmel, S. Ogi, P. Leowanawat and D. Schmidt, *Chem. Rev.*, 2016, **116**, 962–

1052; (*g*) A. Nowak-Król and F. Würthner, *Org. Chem. Front.*, 2019, **6**, 1272–1318.

2 (*a*) K. Peneva, G. Mihov, A. Herrmann, N. Zarrabi, M. Börsch, T. M. Duncan and K. Müllen, *J. Am. Chem. Soc.*, 2008, **130**, 5398–5399; (*b*) C. C. Hofmann, S. M. Lindner, M. Ruppert, A. Hirsch, S. A. Haque, M. Thelakkat and J. Köhler, *J. Phys. Chem. B*, 2010, **114**, 9148–9156; (*c*) F. J. Céspedes-Guirao, A. B. Ropero, E. Font-Sanchis, A. Nadal, F. Fernández-Lázaro and Á. Sastre-Santos, *Chem. Commun.*, 2011, **47**, 8307–8309; (*d*) N. Gálvez, E. J. Kedracka, F. Carmona, F. J. Céspedes-Guirao, E. Font-Sanchis, F. Fernández-Lázaro, Á. Sastre-Santos and J. M. Domínguez-Vera, *J. Inorg. Biochem.*, 2012, **117**, 205–211; (*e*) V. M. Blas-Ferrando, J. Ortiz, L. Bouissane, K. Ohkubo, S. Fukuzumi, F. Fernández-Lázaro and Á. Sastre-Santos, *Chem. Commun.*, 2012, **48**, 6241–6243; (*f*) L. Flamigni, A. Zanelli, H. Langhals and B. Böck, *Photochem. Photobiol. Sci.*, 2013, **12**, 2137–2145; (*g*) M. Marcia, P. Singh, F. Hauke, M. Maggini and A. Hirsch, *Org. Biomol. Chem.*, 2014, **12**, 7045–7058; (*h*) M. Sun, K. Müllen and M. Yin, *Chem. Soc. Rev.*, 2016, **45**, 1513–1528; (*i*) Y. Ye, Y. Zheng, C. Ji, J. Shen and M. Yin, *ACS Appl. Mater. Interfaces*, 2017, **9**, 4534–4539.

3 (*a*) X. Zhan, A. Facchetti, S. Barlow, T. J. Marks, M. A. Ratner, M. R. Wasielewski and S. R. Marder, *Adv. Mater.*, 2011, **23**, 268–284; (*b*) C. Huang, S. Barlow and S. R. Marder, *J. Org. Chem.*, 2011, **76**, 2386–2407; (*c*) C. Li and H. Wonneberger, *Adv. Mater.*, 2012, **24**, 613–636; (*d*) M. Guide, S. Pla, A. Sharenko, P. Zalar, F. Fernández-Lázaro, Á. Sastre-Santos and T.-Q. Nguyen, *Phys. Chem. Chem. Phys.*, 2013, **15**, 18894–18899; (*e*) M. G. Ramírez, S. Pla, P. G. Boj, J. M. Villalvilla, J. A. Quintana, M. A. Díaz-García, F. Fernández-Lázaro and Á. Sastre-Santos, *Adv. Opt. Mater.*, 2013, **1**, 933–938; (*f*) R. Singh, E. Giussani, M. M. Mróz, F. di Fonzo, D. Fazzi, J. Cabanilla-González, L. Oldridge, N. Vaenas, A. G. Kontos, P. Falaras, A. C. Grimsdale, J. Jacob, K. Müllen and P. E. Keivanidis, *Org. Electron.*, 2014, **15**, 1347–1361; (*g*) Z. Xie, B. Xiao, Z. He, W. Zhang, X. Wu, H. Wu, F. Würthner, C. Wang, F. Xie, L. Liu, Y. Ma, W.-Y. Wong and Y. Cao, *Mater. Horiz.*, 2015, **2**, 514–518; (*h*) F. Fernández-Lázaro, N. Zink-Lorre and Á. Sastre-Santos, *J. Mater. Chem. A*, 2016, **4**, 9336–9346; (*i*) L. Gil-Escrig, C. Momblona, D. Forgács, S. Pla, F. Fernández-Lázaro, M. Sessolo, Á. Sastre-Santos and H. J. Bolink, *Org. Electron.*, 2016, **37**, 396–401; (*j*) M. Signoretto, N. Zink-Lorre, I. Suárez, E. Font-Sanchis, Á. Sastre-Santos, V. S. Chirvony, F. Fernández-Lázaro and J. P. Martínez-Pastor, *ACS Photonics*, 2017, **4**, 114–120; (*k*) M. Signoretto, N. Zink-Lorre, J. P. Martínez-Pastor, E. Font-Sanchis, V. S. Chirvony, Á. Sastre-Santos, F. Fernández-Lázaro and I. Suárez, *Appl. Phys. Lett.*, 2017, **111**, 081102; (*l*) P. Clavo-Gredilla, J. García-Calvo, J. V. Cuevas, T. Torroba, J.-L. Pablos, F. C. García, J.-M. García, N. Zink-Lorre, E. Font-Sanchis, Á. Sastre-Santos and F. Fernández-Lázaro, *Chem. – Eur. J.*, 2017, **23**, 13973–13979.

4 (*a*) R. Mishra, J. M. Lim, M. Son, P. Panini, D. Kim and J. Sankar, *Chem. – Eur. J.*, 2014, **20**, 5776–5786; (*b*) G. Rauch and S. Höger, *Chem. Commun.*, 2014, **50**, 5659–5661; (*c*) P. Leowanawat, A. Nowak-Król and F. Würthner, *Org. Chem. Front.*, 2016, **3**, 537–544; (*d*) N. Zink-Lorre, E. Font-Sanchis, Á. Sastre-Santos and F. Fernández-Lázaro, *Dyes Pigm.*, 2016, **127**, 9–17; (*e*) N. Zink-Lorre, E. Font-Sanchis, Á. Sastre-Santos and F. Fernández-Lázaro, *Org. Biomol. Chem.*, 2016, **14**, 9375–9383; (*f*) N. Zink-Lorre, E. Font-Sanchis, Á. Sastre-Santos and F. Fernández-Lázaro, *Org. Chem. Front.*, 2017, **4**, 2016–2021; (*g*) D. Gutiérrez-Moreno, Á. Sastre-Santos and F. Fernández-Lázaro, *Org. Chem. Front.*, 2018, **5**, 1830–1834; (*h*) D. Gutiérrez-Moreno, Á. Sastre-Santos and F. Fernández-Lázaro, *Org. Chem. Front.*, 2019, DOI: 10.1039/C9QO00491B.

5 (*a*) P. Schlichting, B. Duchscherer, G. Seisenberger, T. Basché, C. Bräuchle and K. Müllen, *Chem. – Eur. J.*, 1999, **5**, 2388–2395; (*b*) F. Nolde, J. Qu, C. Kohl, N. G. Pschirer, E. Reuther and K. Müllen, *Chem. – Eur. J.*, 2005, **11**, 3959–3967; (*c*) A. Herrmann and K. Müllen, *Chem. Lett.*, 2006, **35**, 978–985; (*d*) Y. Nagao, T. Iwano, M. Hirano, K. Arimitsu and K. Kozawa, *Heterocycles*, 2012, **84**, 815–828.

6 U. Rohr, P. Schlichting, A. Böhm, M. Gross, K. Meerholz, C. Bräuchle and K. Müllen, *Angew. Chem., Int. Ed.*, 1998, **37**, 1434–1437, (*Angew. Chem.*, 1998, **110**, 1463–1467).

7 J. Calbo, A. Doncel-Giménez, J. Aragó and E. Ortí, *Theor. Chem. Acc.*, 2018, **137**(27), 1–11.

8 (*a*) U. Rohr, C. Kohl, K. Müllen, A. Van de Craats and J. Warman, *J. Mater. Chem.*, 2001, **11**, 1789–1799; (*b*) M. Franceschin, A. Alvino, V. Casagrande, C. Mauriello, E. Pascucci, M. Savino, G. Ortaggi and A. Bianco, *Bioorg. Med. Chem.*, 2007, **15**, 1848–1858; (*c*) I.-H. Lee, Y.-M. Jeon and M.-S. Gong, *Synth. Met.*, 2008, **158**, 532–538; (*d*) Z. An, J. Yu, B. Domercq, S. C. Jones, S. Barlow, B. Kippelen and S. R. Marder, *J. Mater. Chem.*, 2009, **19**, 6688–6698; (*e*) C. L. Eversloh, C. Li and K. Müllen, *Org. Lett.*, 2011, **13**, 4148–4150; (*f*) Q. Yan, K. Cai, C. Zhang and D. Zhao, *Org. Lett.*, 2012, **14**, 4654–4657; (*g*) K. Ida, H. Sakai, K. Ohkubo, Y. Araki, T. Wada, T. Sakanoue, T. Takenobu, S. Fukuzumi and T. Hasobe, *J. Phys. Chem. C*, 2014, **118**, 7710–7720; (*h*) R. Regar, A. R. Sekhar, R. Mishra and J. Sankar, *Indian J. Chem.*, 2018, **57B**, 308–313.

9 (*a*) S. Müller and K. Müllen, *Chem. Commun.*, 2005, 4045–4046; (*b*) Y. Li, H. Zheng, Y. Li, S. Wang, Z. Wu, P. Liu, Z. Gao, H. Liu and D. Zhu, *J. Org. Chem.*, 2007, **72**, 2878–2885; (*c*) W. Jiang, Y. Li, W. Yue, Y. Zhen, J. Qu and Z. Wang, *Org. Lett.*, 2010, **12**, 228–231; (*d*) Y. Li, L. Xu, T. Liu, Y. Yu, H. Liu, Y. Li and D. Zhu, *Org. Lett.*, 2011, **13**, 5692–5695; (*e*) Y. Yang, Y. Wang, Y. Xie, T. Xiong, Z. Yuan, Y. Zhang, S. Qian and Y. Xiao, *Chem. Commun.*, 2011, **47**, 10749–10751; (*f*) J. Kelber, M.-F. Achard, F. Durola and H. Bock, *Angew. Chem., Int. Ed.*, 2012, **51**, 5200–5203; (*g*) Y. Li, W. Xu, S. Di Motta, F. Negri, D. Zhu and Z. Wang, *Chem. Commun.*, 2012, **48**, 8204–8206; (*h*) Z. Zhao, Y. Zhang and Y. Xiao, *J. Org. Chem.*, 2013, **78**, 5544–5549; (*i*) L. Xu, C. Liu, Z. Qin, R. Jiang and Y. Li, *Eur. J. Org. Chem.*, 2013,

300–306; (*j*) X. Zhan, J. Zhang, S. Tang, Y. Lin, M. Zhao, J. Yang, H.-L. Zhang, Q. Peng, G. Yu and Z. Li, *Chem. Commun.*, 2015, **51**, 7156–7159.

10 (*a*) G. Stork and K. Matsuda, *U.S. Patent* 3364275, 1968; *Chem. Abstr.*, 1968, **69**, 10398; (*b*) S. Tokita, K. Hiruta, K. Kitahara and H. Nishi, *Synthesis*, 1982, 229–231; (*c*) C. Göltner, D. Pressner, K. Müllen and H. W. Spiess, *Angew. Chem., Int. Ed. Engl.*, 1993, **32**, 1660–1662; (*d*) S. Alibert-Fouet, I. Seguy, J.-F. Bobo, P. Destruel and H. Bock, *Chem. – Eur. J.*, 2007, **13**, 1746–1753; (*e*) K. V. Rao and S. J. George, *Org. Lett.*, 2010, **12**, 2656–2659; (*f*) E. H. Fort and L. T. Scott, *Tetrahedron Lett.*, 2011, **52**, 2051–2053; (*g*) B. Schuler, S. Collazos, L. Gross, G. Meyer, D. Pérez, E. Guitian and D. Peña, *Angew. Chem., Int. Ed.*, 2014, **53**, 9004–9006.

11 (*a*) H. Langhals and S. Kirner, *Eur. J. Org. Chem.*, 2000, 365–380; (*b*) H. Langhals and P. Blanke, *Dyes Pigm.*, 2003, **59**, 109–116; (*c*) B. Tuesuwan, J. T. Kern, P. W. Thomas, M. Rodríguez, J. Li, W. M. David and S. M. Kerwin, *Biochemistry*, 2008, **47**, 1896–1909; (*d*) J. Kelber, M.-F. Achard, B. Garreau-de Bonneval and H. Bock, *Chem. – Eur. J.*, 2011, **17**, 8145–8155.

12 T. Nakamuro, K. Kumazawa, H. Ito and K. Itami, *Synlett*, 2019, 423–428.

13 F. M. Llogullo, A. H. Seitz and L. Friedman, *Org. Synth.*, 1968, **48**, 12–17.

14 Y. Sato, T. Tamura and M. Mori, *Angew. Chem., Int. Ed.*, 2004, **43**, 2436–2440.

15 Y. Avlasevich, S. Müller, P. Erk and K. Müllen, *Chem. – Eur. J.*, 2007, **13**, 6555–6561.

16 (*a*) R. Webster and M. Lautens, *Org. Lett.*, 2009, **11**, 4688–4691; (*b*) U. K. Tambar and B. M. Stoltz, *J. Am. Chem. Soc.*, 2005, **127**, 5340–5341.

17 M. J. Frisch, G. W. Trucks, H. B. Schlegel, G. E. Scuseria, M. A. Robb, J. R. Cheeseman, G. Scalmani, V. Barone, B. Mennucci, G. A. Petersson, H. Nakatsuji, M. Caricato, X. Li, H. P. Hratchian, A. F. Izmaylov, J. Bloino, G. Zheng, J. L. Sonnenberg, M. Hada, M. Ehara, K. Toyota, R. Fukuda, J. Hasegawa, M. Ishida, T. Nakajima, Y. Honda, O. Kitao, H. Nakai, T. Vreven, J. A. Montgomery Jr., J. E. Peralta, F. Ogliaro, M. Bearpark, J. J. Heyd, E. Brothers, K. Raghavachari, A. Rendell, J. C. Burant, S. S. Iyengar, J. Tomasi, M. Cossi, N. Rega, J. M. Millam, M. Klene, J. E. Knox, J. B. Cross, V. Bakken, C. Adamo, J. Jaramillo, R. Gomperts, R. E. Stratmann, O. Yazyev, A. J. Austin, R. Cammi, C. Pomelli, J. W. Ochterski, R. L. Martin, K. Morokuma, V. G. Zakrzewski, G. A. Voth, P. Salvador, J. J. Dannenberg, S. Dapprich, A. D. Daniels, O. Farkas, J. B. Foresman, J. V. Ortiz, J. Cioslowski and D. J. Fox, *Gaussian 09, Revision D.01*, Gaussian, Inc., Wallingford CT, 2013.

18 (*a*) A. D. Becke, *J. Chem. Phys.*, 1993, **98**, 5648–5652; (*b*) C. T. Lee, W. T. Yang and R. G. Parr, *Phys. Rev. B: Condens. Matter Mater. Phys.*, 1988, **37**, 785–789.

19 M. M. Francl, W. J. Pietro, W. J. Hehre, J. S. Binkley, M. S. Gordon, D. J. DeFrees and J. A. Pople, *J. Chem. Phys.*, 1982, **77**, 3654–3665.

20 G. A. Zhurko, *ChemCraft 1.8*. http://www.chemcraftprog.com.

21 (*a*) C. Jamorski, M. E. Casida and D. R. Salahub, *J. Chem. Phys.*, 1996, **104**, 5134–5147; (*b*) M. E. Casida, C. Jamorski, K. C. Casida and D. R. Salahub, *J. Chem. Phys.*, 1998, **108**, 4439–4449; (*c*) M. Petersilka, U. J. Gossmann and E. K. U. Gross, *Phys. Rev. Lett.*, 1996, **76**, 1212–1215.